The Rab GTPase activating protein TBC-2 regulates endosomal localization of DAF-16 FOXO and lifespan

İçten Meraş[1,2,3], Laëtitia Chotard[2,4], Thomas Liontis[3,5,6], Zakaria Ratemi[3], Benjamin Wiles[3], Jung Hwa Seo[3], Jeremy M. Van Raamsdonk[3,4,5,6] and Christian E. Rocheleau[1,2,3,4]*

[1]Department of Anatomy and Cell Biology, McGill University, Montreal, Canada; [2]Division of Endocrinology and Metabolism, Department of Medicine, McGill University, Montreal, Canada; [3] Metabolic Disorders and Complications Program, Centre for Translational Biology, Research Institute of the McGill University Health Centre, Montreal, Canada; [4]Division of Experimental Medicine, Department of Medicine, McGill University, Montreal, Canada; [5]Department of Neurology and Neurosurgery, McGill University, Montreal, Canada; [6]Brain Repair and Integrative Neuroscience Program, Centre for Translational Biology, Research Institute of the McGill University Health Centre, Montreal, Canada

*Correspondence: Christian E. Rocheleau (christian.rocheleau@mcgill.ca)

Running title: Endosomal Regulation of FOXO transcription factors

ABSTRACT

FOXO transcription factors have been shown to regulate longevity in model organisms and are associated with longevity in humans. To gain insight into how FOXO functions to increase lifespan, we examined the subcellular localization of DAF-16 in *C. elegans.* We show that DAF-16 is localized to endosomes and that this endosomal localization is increased by the insulin-IGF signaling (IIS) pathway. Endosomal localization of DAF-16 is modulated by endosomal trafficking proteins. Disruption of the Rab GTPase activating protein TBC-2 increases endosomal localization of DAF-16, while inhibition of TBC-2 targets, RAB-5 or RAB-7 GTPases, decreases endosomal localization of DAF-16. Importantly, the amount of DAF-16 that is localized to endosomes has functional consequences as increasing endosomal localization through mutations in *tbc-2* reduced the lifespan of long-lived *daf-2 IGFR* mutants, depleted their fat stores, and DAF-16 target gene expression. Overall, this work identifies endosomal localization as a mechanism regulating DAF-16 FOXO, which is important for its functions in metabolism and aging.

35 **INTRODUCTION**

36 Insulin/insulin-like growth factor signaling (IIS) is an evolutionarily conserved pathway
37 that plays an important role in lifespan, development, metabolism, immunity and stress responses
38 from *Caenorhabditis elegans* to humans (Accili and Arden, 2004; Barthel *et al.*, 2005; Greer and
39 Brunet, 2005; Murphy and Hu, 2013). IIS-mediated regulation of *C. elegans* FOXO, DAF-16,
40 was first identified via genetic characterization of mutants affecting dauer (an alternative stress
41 resistant larval stage) and life span (Riddle *et al.*, 1981; Kenyon *et al.*, 1993; Lin *et al.*, 1997;
42 Ogg *et al.*, 1997). For example, animals that have a mutation in their insulin-like growth factor
43 receptor (IGFR), DAF-2, live almost two times longer than wild type animals in a DAF-16-
44 dependent manner (Kenyon *et al.*, 1993). Under favorable conditions, the *C. elegans* DAF-2
45 IGFR signals through a conserved PI3K/Akt pathway to phosphorylate and inhibit nuclear
46 accumulation of DAF-16 FOXO (Murphy and Hu, 2013). In short, DAF-2 IGFR activation
47 leads to the activation of AGE-1 PI3K which phosphorylates PI(4,5)P_2 to generate PI(3,4,5)P_3,
48 which can bind and recruit PDK-1 and AKT-1/2 kinases. DAF-18 PTEN, a lipid and protein
49 phosphatase, countacts AGE-1 PI3K and thus negatively regulates signaling. PDK-1 activates
50 AKT-1/2 which in turn phosphorylates DAF-16 creating binding sites for PAR-5 and FTT-2 14-
51 3-3 scaffold proteins that sequester DAF-16 FOXO in the cytoplasm. During adverse conditions
52 such as starvation, IIS is suppressed and DAF-16 FOXO enters the nucleus to induce the
53 expression of stress response genes. As such, DAF-16 FOXO mediates most *daf-2 IGFR* mutant
54 phenotypes.

55 Upon activation, the Insulin/IGF receptor is internalized into endosomes, where it can
56 disassociate from its ligand and recycle back to the plasma membrane, or it can be targeted for
57 lysosomal degradation (Bergeron *et al.*, 2016). The identification of activated IGFR on

58 endosomes suggested that endosomes can serve as a platform for signaling (Baass *et al.*, 1995).
59 Subsequently, several components of the IIS pathway have been shown to localize on
60 endosomes. PTEN localizes on PI(3)P positive endosomes through its C2 domain and has been
61 demonstrated to regulate endosome trafficking via dephosphorylation of Rab7 (Naguib *et al.*,
62 2015; Shinde and Maddika, 2016). Akt2 localizes to Appl-1 and WDFY-2 positive endosomes to
63 get fully activated and regulate Akt2 specific downstream substrates (Schenck *et al.*, 2008; Walz
64 *et al.*, 2010). 14-3-3 proteins can interact with several Akt phosphorylation targets to regulate
65 their subcellular localization and have been found on endosomes (Jungmichel *et al.*, 2014; Marat
66 *et al.*, 2017). However, a role for endosome trafficking in regulation of FOXO transcription
67 factors has not been demonstrated to the best of our knowledge.

68 Rab5 and Rab7 GTPases localize to early and late endosomes respectively and are critical
69 regulators of trafficking to the lysosome, an organelle important for cargo degradation and
70 metabolic signaling (Huotari and Helenius, 2011; Settembre *et al.*, 2013). Like many small
71 GTPases, Rabs cycle between a GTP-bound active state and GDP-bound inactive state. This
72 cycling requires guanine nucleotide exchange factors for activation and GTPase Activating
73 Proteins (GAPs) to catalyze GTP hydrolysis and hence Rab inactivation. We previously
74 characterized *C. elegans* TBC-2 as having *in vitro* GAP activity towards RAB-5, and some
75 activity towards RAB-7 (Chotard *et al.*, 2010a). Mutations in *tbc-2* result in enlarged late
76 endosomes in several tissues including the intestine, an important site of IIS and metabolic
77 regulation (Libina *et al.*, 2003). In addition to early to late endosome maturation, TBC-2
78 regulates phagosome maturation (Li *et al.*, 2009), dense core vesicle maturation (Sasidharan *et*
79 *al.*, 2012) endosome recycling as an effector of RAB-10 and CED-10/Rac (Sun *et al.*, 2012; Liu
80 and Grant, 2015) and yolk protein trafficking in oocytes and embryos (Chotard *et al.*, 2010b).

81 Yolk protein is prematurely degraded in *tbc-2* mutants. As such, *tbc-2* mutant larvae hatched in
82 the absence of food had reduced survival during L1 (first larval stage) diapause (Chotard *et al.*,
83 2010b).

84 Here we explore the subcellular localization of DAF-16 and show that DAF-16 localizes
85 on early and late endosomes in *C. elegans* intestinal cells. We found that endosome localization
86 of DAF-16 is regulated by nutrient availability and IIS. We show that endosome localization of
87 DAF-16 is increased through mutations in *tbc-2*, at the expense of nuclear localization. The
88 increased endosomal localization of DAF-16 in *tbc-2* mutants decreases lifespan, fat storage and
89 DAF-16 target gene expression in *daf-2 IGFR* mutant animals. These results demonstrate a role
90 of endosomal localization in the regulation and function of DAF-16 FOXO.

91

92

93 **RESULTS**
94

95 **TBC-2 and the RAB-5 and RAB-7 GTPases regulate DAF-16 localization to endosomes in**
96 **the intestine**

97 We previously reported that *tbc-2* is required for survival during L1 diapause (Chotard *et*
98 *al.*, 2010b). Since *daf-16* is also required for survival during L1 diapause (Munoz and Riddle,
99 2003; Baugh and Sternberg, 2006) we sought to test whether TBC-2 might regulate the nuclear
100 versus cytoplasmic localization of DAF-16. Although we determined that loss of *tbc-2* did not
101 result in precocious development during L1 diapause as seen *daf-16* mutants (Baugh and
102 Sternberg, 2006; Chotard *et al.*, 2010b), we found that TBC-2 does in fact regulate DAF-16
103 localization. Unexpectedly, we found that DAF-16a::GFP (*zIs356*) localized to numerous
104 amorphous vesicles in the intestinal cells of *tbc-2(tm2241)* deletion mutant animals (Figure 1B).
105 Furthermore, we found that DAF-16a::GFP localized to cytoplasmic vesicles in the intestine of
106 wild-type animals (Figure 1A). The percentage of hermaphrodites with DAF-16 vesicles
107 increased during larval development, peaking at L4 and young adults (Figure 1I, Figure 1 -
108 figure supplement 1A). *tbc-2(tm2241)* animals were about twice as likely to have DAF-16
109 vesicles than wild-type (Figure 1J, Figure 1 - figure supplement 1A). The number of DAF-16
110 positive vesicles in wild-type can range from zero to hundreds (Figure 1I). Vesicles can be
111 distributed throughout all 20 intestinal cells or be present in high numbers in just a few cells.
112 DAF-16a::GFP localization is not sex specific as we found similar numbers of DAF-16 positive
113 vesicles in males as in hermaphrodites (Figure 1 - figure supplement 1B). Although DAF-
114 16a::GFP nuclear localization is low in normal growth conditions, we find that *tbc-2(tm2241)*
115 intestinal nuclei appear to have less nuclear DAF-16a::GFP than wild-type (Figure 1A and B).
116 We quantified the fluorescence intensity of DAF-16a::GFP in nuclei of *tbc-2(tm2241)* intestinal

117 cells comparing nuclei of cells with vesicles versus nuclei of cells without vesicles (Figure 1K).
118 We found that nuclei of cells with vesicles have significantly less nuclear DAF-16a::GFP than
119 cells without vesicles. Thus, DAF-16 localizes to vesicles in wild-type and *tbc-2(tm2241)*
120 animals, and *tbc-2(tm2241)* animals have less nuclear DAF-16a::GFP, likely due to sequestration
121 to cytoplasmic vesicles.

122 To determine if the localization of the GFP tag or the splice variant or expression levels
123 affected DAF-16 vesicular localization we analyzed three other transgenic strains with lower
124 expression levels; GFP::DAF-16a (*muIs71*), DAF-16a::RFP (*lpIs12*) and DAF-16f::GFP (*lpIs14,*
125 with an alternative N-terminus)(Henderson and Johnson, 2001; Lin *et al.*, 2001; Kwon *et al.*,
126 2010). Using the three fluorescent reporters, we detected DAF-16 vesicles in the *tbc-2(tm2241)*
127 mutant, albeit not in the wild-type background (Figure 1 – figure supplement 2G-X).
128 Overexpression of GFP from *vha-6* intestinal specific promoter, *vhEx1[Pvha-6::GFP]*, did not
129 show significant vesicular localization in wild-type animals (Figure 1 – figure supplement 3A).
130 In *tbc-2(tm2241)* animals GFP showed some vesicular localization and potential aggregates, but
131 much less than seen with DAF-16a::GFP, indicating that the vesicular localization is due to
132 DAF-16 and not the GFP tag. Of note, we found that GFP expression in the *tbc-2* background
133 was visibly stronger than in wild-type (Figure 1 – figure supplement 3B-E), consistent with *vha-*
134 *6* ranking amongst the top downregulated DAF-16-responsive genes (Tepper *et al.*, 2013) and
135 consistent with TBC-2 facilitating DAF-16 nuclear localization.

136 To determine if endogenous DAF-16 localizes to vesicles we analyzed *daf-16(hq23)*, a
137 DAF-16::GFP line generated by CRISPR/Cas9 genome editing (Zhang *et al.*, 2021), and found
138 that endogeneously tagged DAF-16 localized to vesicles in both wild-type and *tbc-2(tm2241)*
139 mutants (Figure 1 – figure supplement 2A-F). To determine if the GFP/RFP tag is driving

140 vesicular localization of DAF-16 we analyzed two *daf-16* alleles endogenously tagged with
141 evolutionarily distant mNeongreen and mKate2 fluorescent proteins (Bhattacharya *et al.*, 2019;
142 Aghayeva *et al.*, 2020). We found that DAF-16::mNG and DAF-16::mK2 both localized to
143 intestinal vesicles in wild-type animals (Figure 2). Furthermore, the percent wild-type and *tbc-*
144 *2(tm2241)* animals with endogenous DAF-16::mNG vesicles were comparable to that of the
145 overexpressed DAF-16a::GFP (Figure 2I). Therefore, DAF-16 localization to vesicles is not due
146 to overexpression and unlikely to be an artifact of the fluorescent tag.
147 The finding that DAF-16 localizes to enlarged vesicles in *tbc-2* mutants and that DAF-16
148 vesicles contain autofluorescent material (Figure 1E-H, Figure 2E,F), a hallmark of intestinal
149 endolysosomes (Clokey and Jacobson, 1986; Hermann *et al.*, 2005; Coburn *et al.*, 2013),
150 suggested that DAF-16 vesicles are endosomal. To determine if the DAF-16 vesicles are
151 endosomes, we co-expressed DAF-16a::GFP with RFP::RAB-5, an early endosomal marker, or
152 with mCherry::RAB-7, a late endosomal marker (Chavrier *et al.*, 1990; Sato *et al.*, 2005; Chen *et*
153 *al.*, 2006). We found that in wild-type animals, DAF-16a::GFP localizes to a subset of RAB-5
154 and RAB-7-positive endosomes (Figure 3A-F). Thirty percent of DAF-16a::GFP vesicles were
155 RAB-5 positive (n=959) while 5% were RAB-7 positive (n=365). Furthermore, we tested the
156 genetic requirements for *rab-5* and *rab-7* for DAF-16 localization by RNAi. We found that *rab-*
157 *5(RNAi)* and *rab-7(RNAi)* knockdown significantly decreased the number of wild-type and *tbc-*
158 *2(tm2241)* animals with DAF-16a::GFP vesicles (Figure 3G and H). Together, these data are
159 consistent with DAF-16 localizing to a sub-population of endosomes or endosome-like vesicles
160 in the intestinal cells. It further implicates endosomal regulators TBC-2, RAB-5 and RAB-7 as
161 regulators of DAF-16.
162

163 **Acute starvation suppresses DAF-16 localization to endosomes**

164 Nuclear localization of DAF-16 is modulated by nutrient availability. As such, starvation
165 promotes DAF-16 cytoplasmic-to-nuclear shuttling (Henderson and Johnson, 2001). To
166 determine if endosomal DAF-16 can translocate to the nucleus, we tested the effect of acute
167 starvation on DAF-16a::GFP localization to endosomes. We found that starvation strongly
168 suppressed the localization of DAF-16 to endosomes in both wild-type and *tbc-2(tm2241)*
169 mutants (Figure 4A; Figure 4 – figure supplement 1). Upon re-feeding, DAF-16 relocalized to
170 endosomes after 1-2 hours, in both wild-type and *tbc-2(tm2241)* mutants. Thus, DAF-16
171 localization on endosomal membranes is regulated by nutrient availability.

172

173 **Insulin/IGF signaling regulates DAF-16 localization to endosomes**

174 To determine if IIS regulates DAF-16 localization to endosomes we analyzed the effect
175 of disrupting IIS on DAF-16a::GFP localization (see Figure 4B for reference). Firstly, we
176 analyzed a hypomorphic mutant of the insulin/IGF receptor, *daf-2(e1370)*, in which IIS is
177 reduced, particularly at higher temperatures (Swanson and Riddle, 1981). We compared DAF-
178 16a::GFP localization in three independent *daf-2(e1370)* strains at 15°C and shifted overnight to
179 25°C to enhance disruption of DAF-2. All three showed a significant reduction in the number of
180 DAF-16 positive vesicles at 25°C, while the wild-type strain did not (Figure 3C), indicating that
181 DAF-2 promotes DAF-16 localization to endosomes.

182 DAF-18, the homolog of human tumor suppressor protein PTEN, acts as a negative
183 regulator of the IIS pathway counteracting AGE-1 PI3K signaling by dephosphorylating the
184 3'phosphate on the PI(3,4,5)P_3 converting it to PI(4,5)P_2 (Ogg and Ruvkun, 1998). We analyzed
185 DAF-16a::GFP localization in the *daf-18* reference allele, *e1375.* We generated three

186 independent *daf-18(e1375); zIs356* strains, but only two strains had increased endosome
187 localization of DAF-16. However, combined data from the three strains had a statistically
188 significant increase in the number of animals with DAF-16 endosomes (Figure 4D). Since *daf-*
189 *18(e1375)* is possibly a non-null allele, we analyzed a deletion allele, *daf-18(ok480).* We found
190 that five independent *daf-18(ok480); zIs356* strains had more DAF-16 endosomes than wild-type
191 that when combined was statistically significant (Figure 4D). Since DAF-16 endosome
192 localization is mildly increased in the background of two distinct *daf-18* alleles, it is consistent
193 with increased IIS causing an increase in DAF-16 localization to endosomes.

194 *C. elegans* AKT-1 and AKT-2 function upstream of, and can phosphorylate, DAF-16
195 (Paradis and Ruvkun, 1998; Hertweck *et al.*, 2004). The SGK-1 Serum Glucorticoid Kinase
196 homolog interacts with AKT kinases and has been shown to regulate DAF-16 nuclear
197 localization (Hertweck *et al.*, 2004). We tested which of these kinases might regulate DAF-16
198 localization to endosomes. We found that animals with an *akt-2(ok393)* deletion mutation, there
199 was an insignificant decrease in DAF-16 endosomal localization in two independent strains
200 (Figure 4E). However, in *akt-1*(*RNAi)* animals, we observed a significant decrease in DAF-16
201 endosomal localization where DAF-16 localized mainly to the nucleus, compared to the control
202 animals in three independent experiments (Figure 4F). Neither an *sgk-1(ok538)* deletion nor an
203 *sgk-1(ft15)* gain-of-function allele affected DAF-16 localization to endosomes (Hertweck *et al.*,
204 2004; Jones *et al.*, 2009)(Figure 4G). Therefore, AKT-1 is the main kinase regulating DAF-16
205 localization to endosomes.

206 Phosphorylation of FOXO proteins by Akt creates binding sites for 14-3-3 proteins,
207 which promote cytoplasmic retention of FOXO (Brunet *et al.*, 1999). *C. elegans* has two genes
208 that encode for 14-3-3 proteins that interact with DAF-16, *par-5* and *ftt-2* (Wang and Shakes,

209 1997; Morton *et al.*, 2002; Wang *et al.*, 2006). We found that *ftt-2(RNAi)*, but not *par-5(RNAi)*,
210 suppressed the localization of DAF-16 to endosomes (Figure 4H), suggesting that FTT-2
211 regulates DAF-16 endosomal localization.

212 To determine if AKT phosphorylation regulates DAF-16 localization to endosomes we
213 tested if DAF-16a^{AM}::GFP *muIs113*, in which the four consensus AKT phosphorylation sites
214 (T54A, S240A, T242 and S314A) are mutated to alanine (Lin *et al.*, 2001), could still localize to
215 vesicles in *tbc-2(tm2241)* mutants. Since the expression levels are lower than DAF-16a::GFP
216 *zIs356*, we used GFP::DAF-16a *muIs71* with comparable expression levels as control (Figure 4 –
217 figure supplement 2). We found that the number of *tbc-2(tm2241)* animals with DAF-
218 16a^{AM}::GFP positive vesicles was significantly less than the GFP::DAF-16a control (Figure 4I).
219 Together, these data demonstrate that IIS regulates endosomal DAF-16 through AKT-1 specific
220 phosphorylation and FTT-2 14-3-3.

221

222 **TBC-2 is required for lifespan extension and increased fat storage of *daf-2(e1370)* mutants**

223 To determine if the increased endosomal localization of DAF-16 seen in *tbc-2* mutants
224 affects DAF-16 activity, we tested if TBC-2 regulates adult lifespan. We found that the *tbc-*
225 *2(sv41)* and *tbc-2(tm2241)* deletion alleles had similar lifespans as compared to wild-type
226 (Figure 5A and B; Figure 5 – figure supplement 1). As expected, *daf-2(e1370)* animals lived
227 significantly longer than wild-type. We found that both *tbc-2* alleles significantly shortened the
228 lifespan of *daf-2(e1370)* animals (Figure 5A and B; Figure 5 – figure supplement 1). Thus,
229 TBC-2 is not required for normal lifespan, but is partly required for the extended lifespan of *daf-*
230 *2(e1370)* mutants.

231 To assess TBC-2's contribution to other *daf-2* mutant phenotypes, we tested whether
232 TBC-2 is required for the increased fat storage of *daf-2(e1370)* mutants. Consistent with
233 previous findings we found that *daf-2(e1370)* had significantly more fat than wild-type animals
234 as determined by Nile Red and Oil Red O staining of fixed L4 larvae (Kimura *et al.*, 1997;
235 O'Rourke *et al.*, 2009) (Figure 5C-F). We found that *tbc-2(tm2241)* larvae had less fat than wild-
236 type with Nile Red staining, but not with Oil Red O staining (Figure 5D and F). This difference
237 might reflect the lower sensitivity of Oil Red O for quantifying lipid abundance as compared to
238 Nile Red (Escorcia *et al.*, 2018). Interestingly, we found that *tbc-2(tm2241)* significantly
239 suppressed the *daf-2(e1370)* increased lipid staining by both Nile Red and Oil Red O (Figure 5C-
240 F). Thus, TBC-2 is required for the increased fat storage of *daf-2(e1370)* mutants.
241 The fact that TBC-2 is required for the increased longevity and increased fat storage of
242 *daf-2(e1370)* mutants suggests that TBC-2 could be a negative regulator of IIS. Therefore, we
243 tested if *tbc-2* mutants regulate DAF-16 target gene expression in *daf-2(e1370)* animals. We
244 used qRT-PCR to measure the expression of DAF-16 target genes in wild-type, *daf-2(e1370),*
245 *tbc-2* mutants and *tbc-2; daf-2* double mutants. Consistent with previous reports, the expression
246 of six of the DAF-16 target genes were upregulated in *daf-2(e1370)* animals (Figure 6) (Honda
247 and Honda, 1999; Murphy *et al.*, 2003; Ackerman and Gems, 2012; Tepper *et al.*, 2013). While
248 *tbc-2(tm2241)* and *tbc-2(sv41)* did not appreciably alter DAF-16 target gene expression relative
249 to wild-type, both reduced the expression of *sod-3, dod-3, gpd-2* and *icl-1* in *daf-2(e1370)*
250 mutants, while *mtl-1* and *ftn-1* were not significantly decreased (Figure 6). The fact that TBC-2
251 was required for the increased expression of four of six DAF-16 target genes with elevated
252 expression in *daf-2(e1370)* mutants suggests a more specific role for TBC-2 in regulating DAF-2
253 to DAF-16 signaling.

254

255

256 **DISCUSSION**

257 Endosome trafficking and signal transduction are intimately linked processes regulating signal
258 propagation, specificity and attenuation (Miaczynska, 2013; Bergeron *et al.*, 2016). However,
259 there remains a large knowledge gap in the spatial regulation of cell signaling and where
260 downstream transcription factors are regulated. We identified a previously unknown localization
261 for the DAF-16 FOXO transcription factor on endosomes in *C. elegans*. Endosome localization
262 is limited by the TBC-2 Rab GAP. Loss of *C. elegans* TBC-2 results in increased endosomal
263 localization of DAF-16 at the expense of nuclear localization. As such, *C. elegans* TBC-2 is
264 partly required for several *daf-2 IGFR* mutant phenotypes including lifespan extension, increased
265 fat storage, and increased DAF-16 target gene expression that result from DAF-16 nuclear
266 translocation. DAF-16 endosome localization is largely dependent on IIS consistent with this
267 being a phosphorylated, inactive pool of DAF-16. Together our data show a role for the TBC-2
268 Rab GAP in regulating the balance of nuclear versus endosomal localization of the DAF-16
269 transcription factor.

270

271 **DAF-16 localizes to endosomes**

272 We were surprised to find that DAF-16 FOXO localizes to a subset of RAB-5 and RAB-7
273 endosomes in wild-type animals. Many studies have used DAF-16 cytoplasmic versus nuclear
274 localization to assess IIS activity under various conditions. We assume that DAF-16 positive
275 endosomes were not discovered earlier as nuclear translocation can be assessed at low
276 magnification where DAF-16 positive endosomes are not apparent, and DAF-16 positive

277 endosomes are not present in every cell or every animal. Furthermore, we first took notice of
278 DAF-16 positive endosomes in the *tbc-2* mutant background where they are more prominent.
279 These are likely not an artefactual consequence of overexpression, as we see these vesicles in the
280 endogenously tagged *daf-16::GFP* and we do not see similar vesicles in a GFP overexpression
281 strain. DAF-16::mNG and DAF-16::mK2 also localize to vesicles indicating that membrane
282 localization is unlikely to be an artifact of the GFP tag. Additionally, DAF-16-vesicles are
283 regulated by IIS.

284 Many components of the IIS pathway localize to endosomes in mammalian cells
285 including active insulin receptor and downstream signaling components such as PI3K, Akt,
286 PTEN and 14-3-3 proteins (Khan *et al.*, 1986; Christoforidis *et al.*, 1999; Balbis *et al.*, 2000;
287 Braccini *et al.*, 2015; Naguib *et al.*, 2015; Bergeron *et al.*, 2016; Marat *et al.*, 2017; Kim *et al.*,
288 2018). In the case of Akt and PTEN, both have demonstrated roles in regulation of endosome
289 trafficking independent of IIS (Shinde and Maddika, 2016, 2017; Mondin *et al.*, 2019; Hsu *et al.*,
290 2020). On the other hand, the PI3Ks are Rab5 effectors and Rab5 has been shown to promote
291 Akt activity on endosomes (Christoforidis *et al.*, 1999; Shin *et al.*, 2005; Su *et al.*, 2006; Cheng
292 *et al.*, 2009; Braccini *et al.*, 2015). While endosomal localization of FOXO proteins has not been
293 reported to the best of our knowledge, knockdown of Rab5 in mouse liver results in a strong
294 increase in phosphorylated FOXO1 (Zeigerer *et al.*, 2015). This is contrary to the finding that
295 Rab5 promotes Akt phosphorylation (Su *et al.*, 2006; Braccini *et al.*, 2015), which could be a
296 consequence of indirect regulation or suggest tissue-specific regulation. The fact that TBC-2 is a
297 RAB-5 GAP is consistent with increased RAB-5 activity promoting DAF-16 localization on
298 endosomes. This is further supported by the fact that *rab-5* and *rab-7* RNAi knockdown reduces
299 the number of animals with DAF-16 vesicles in both wild-type and *tbc*-2 mutants. Given the

300 importance of RAB-5 for endosome trafficking, it is difficult to parse whether RAB-5 is
301 promoting a platform for DAF-16 localization or if it also has a role in IIS.
302 We demonstrated that DAF-16 localized to a subset of RAB-5 and RAB-7 positive
303 endosomes. Since RAB-5 and RAB-7 promote trafficking to the lysosome and promote receptor
304 tyrosine kinase degradation, it is possible that DAF-16-positive endosomes are signaling
305 endosomes, in which case we would expect other upstream signaling components might be
306 present. Consistent with that hypothesis, knockdown of IIS reduces the number of animals with
307 DAF-16 vesicles. However, when analyzing DAF-16 localization in *daf-2(e1370)* mutants at
308 15°C vs. 25°C, we find that while there is a reduction in the number of DAF-16 endosomes,
309 these endosomes are noticeably fainter at 25°C. This suggests that there are not necessarily less
310 endosomes being generated, but rather less DAF-16 on the vesicles which may be inconsistent
311 with these being signaling endosomes derived from DAF-2 internalization at the plasma
312 membrane. On the other hand, the fact that Akt and 14-3-3 can localize to endosomes in
313 mammalian cells (Balbis *et al.*, 2000; Braccini *et al.*, 2015; Marat *et al.*, 2017) and that AKT-1
314 and FTT-2 promote DAF-16 localization to endosomes, suggests that these proteins might recruit
315 DAF-16 onto endosomes rather than DAF-16 interacting directly with membranes. Future
316 studies should test whether DAF-2 IGFR and downstream IIS components actively recruit DAF-
317 16 to endosomes or whether IIS has a passive role. IIS inhibition of nuclear DAF-16 could result
318 in increased DAF-16 in the cytoplasm where it can bind endosomes.
319 If these are not signaling endosomes, then what are the DAF-16 endosomes? Since
320 RAB-5 and RAB-7 are also regulators of autophagy, so it is possible that these endosomes
321 contribute to degradation of inactive excess DAF-16. There is precedent for selective autophagy
322 in the degradation of the GATA4 transcription factor (Kang *et al.*, 2015). Alternatively, these

323 endosomes could serve as a reservoir of inactive DAF-16 that can be quickly mobilized if
324 environmental stress is encountered. For example, we found that acute starvation is a potent
325 regulator of DAF-16 endosome localization, even in the *tbc-2* mutant background.
326 We find it interesting that there is such variability within the population, and amongst the
327 intestinal cells in a given animal, as to whether there will be DAF-16 positive endosomes or not.
328 It suggests that each intestinal cell autonomously senses changes in IIS, or possibly other nutrient
329 and stress sensing pathways, to regulate DAF-16 localization. Then, why is endosomal DAF-16
330 more prominent in *tbc-2* mutants? One explaination would be that the expansion of endosomal
331 membranes in a *tbc-2* mutant create more storage space for inactive DAF-16. Another would be
332 that IIS or other pathways are more active in *tbc-2* mutants, or some combination of the two.
333 GLP-1/Notch signaling in the germline, AMPK, JNK and LET-363/mTor signaling additionally
334 regulate DAF-16 and could be subject to regulation by TBC-2, particularly mTor which localizes
335 to lysosomes (Oh *et al.*, 2005; Berman and Kenyon, 2006; Greer *et al.*, 2007; Sancak *et al.*,
336 2008; Robida-Stubbs *et al.*, 2012; Sun *et al.*, 2017).
337

338 **A direct role for TBC-2 in regulating *daf-2(e1370) IGFR* mutant phenotypes**

339 Our finding that *tbc-2* was required for the extended lifespan and increased fat storage of *daf-*
340 *2(e1370)* mutants suggests that TBC-2 might have a more specific role related to IIS. However,
341 TBC-2 is not the first endosomal regulator required for lifespan extension of *daf-2(e1370)*
342 mutants. *C. elegans* BEC-1, a homolog of human Beclin1, is a regulator of autophagy and
343 endosome trafficking, and *bec-1* mutants accumulate large late endosomes in the intestinal cells
344 (Melendez *et al.*, 2003; Ruck *et al.*, 2011; Law *et al.*, 2017). Mutations in *bec-1* suppress the
345 increased lifespan of *daf-2(e1370)*, and were reported to be required for the increased fat storage

346 (Melendez *et al.*, 2003). Similarly, other autophagy regulators, *atg-7* and *atg-12*, have been
347 shown to be required for *daf-2* longevity (Hars *et al.*, 2007). An RNAi screen identified
348 regulators of endosome to lysosome trafficking, including RAB-7, and components of the
349 ESCRT and HOPS complexes as being required for the lifespan extension phenotypes of *daf-2*
350 *IGFR* mutants (Samuelson *et al.*, 2007). However, the mechanisms by which they regulate
351 lifespan are not known. In *daf-2(e1370)* mutants, there is an increase in autophagy and lysosome
352 function, both of which are required for the extended lifespan (Melendez *et al.*, 2003; Lapierre *et*
353 *al.*, 2013; Guo *et al.*, 2014; Sun *et al.*, 2020), consistent with increased stress resistance
354 contributing to increased longevity. Since the human homologs of TBC-2 are implicated in
355 autophagy (Behrends *et al.*, 2010; Popovic *et al.*, 2012; Carroll *et al.*, 2013; Toyofuku *et al.*,
356 2015), and *tbc-2* mutants accumulate autophagy protein LGG-1 (LC3/Atg8) in enlarged
357 endosomes (Chotard *et al.*, 2010a), it is possible that TBC-2 also regulates autophagy and thus
358 *daf-2(-)* longevity. However, our findings that TBC-2 regulates DAF-16 nuclear vs. endosome
359 localization and that TBC-2 is required for the DAF-16 target gene expression in *daf-2* mutants
360 demonstrate that TBC-2 has a more direct role in IIS, as opposed to being required for
361 downstream cellular responses. It will be interesting to test if TBC-2 regulates DAF-16-
362 independent mechanisms of longevity as well as to determine if other endosome and autophagy-
363 regulating genes can regulate DAF-16 localization to endosomes.

364 In conclusion, we demonstrate that the DAF-16 FOXO transcription factor localizes to
365 endosomes. This endosomal localization of DAF-16 FOXO is regulated by both IIS and the
366 TBC-2 family of Rab5 and Rab7 GAPs. TBC-2 promotes the nuclear localization of DAF-16
367 FOXO, and this localization has functional effects on both longevity and metabolism through
368 modulation of DAF-16 target gene expression. Our data suggest that endosomes serve as an

369 important location for DAF-16 FOXO transcription factor regulation, and suggest that
370 endomembranes may function as a site of transcription factor regulation.
371
372 **METHODS**
373
374 ***C. elegans* genetics and strain construction**
375 *C. elegans* strains were cultured as described in Wormbook (www.wormbook.org). The *C.*
376 *elegans* N2 Bristol strain was the wild-type parent strain and HB101 *E. coli* strain was used as a
377 food source. Both were obtained from the Caenorhabditis Genetic Center (CGC) as were many
378 of the strains used in this study (Key Resource Table). New strains were constructed using
379 standard methods and the presence of mutations were confirmed by PCR and DNA sequencing.
380
381 **RNAi experiments**
382 *C. elegans* RNAi feeding experiments were conducted essentially as described in (Kamath *et al.*,
383 2001). RNAi feeding clones were obtained from the Ahringer RNAi library and confirmed by
384 sequencing (Key resources table)(Fraser *et al.*, 2000; Kamath *et al.*, 2003). The L4440 empty
385 RNAi feeding vector transformed into HT115(DE3) was used as a negative control (Timmons
386 and Fire, 1998).
387
388 **Microscopy**
389 DAF-16 vesicular localization was analyzed in the intestinal cells of hermaphrodites.
390 Hermaphrodite worms at the L4 stage were imaged alive at room temperature unless it is stated

391 otherwise. Animals were picked and mounted onto 4% agarose pads, animals were anesthetized
392 with levamisole.

393 Differential interference contrast (DIC) and fluorescent imaging were performed with an
394 Axio Imager A1 compound microscope with a 100×1.3 NA Plan-Neofluar oil-immersion
395 objective lens (Zeiss) and images were captured by using an Axio Cam MRm camera and
396 AxioVision software (Zeiss). Confocal microscopy was performed on an Axio Observer Z1
397 LSM780 laser scanning confocal microscopes with a 63×1.4 NA Plan-Apochromat oil-
398 immersion objective lens (Zeiss) in a multi-track mode using an argon multiline laser (405 nm
399 excitation for autofluoresence, 488 nm excitation for GFP and a 561/ 594 nm excitation for
400 mCherry/RFP). Images were captured with a 32 channel GaAsP detector and ZEN2010 image
401 software. Raw data was analyzed using Fiji (ImageJ) or Zen 2010 Lit programs, and images were
402 modified by using Fiji (ImageJ).

403 To compare DAF-16 (*zIs356*) nuclear intensity in cells with or without DAF-16 vesicles,
404 animals at L4 stage were imaged using an LSM780 scanning laser microscope. To ensure
405 consistency, only the anterior most intestine cells were imaged. First, the nucleus of intestinal
406 cells were focused under bright field and without changing the position, GFP, autofluoresence
407 and bright field signals were imaged. Each animal was imaged using the same confocal settings.
408 After data collection, each nucleus was categorized as a nucleus with adjacent DAF-16-positive
409 vesicles or a nucleus without any DAF-16 positive vesicles. Total GFP intensity inside the
410 nucleus was measured using Fiji (Image J) software. The nucleus is circled using DIC/Bright
411 Field and autofluorescence channels as reference. Since intestinal cells have two nuclei per cells,
412 if there are two nuclei within the focus, their GFP intensity is averaged for statistical analysis.

413 Prism 8 (GraphPad) were used to graph the data and determine statistical analysis using an
414 unpaired t-test.
415
416 **Starvation-Refeeding and Temperature Shift Experiments**
417 For starvation and refeeding experiments animals were synchronized at the L1 stage and grown
418 NGM plates with HB101 *E. coli* till the L4 stage. Then animals were collected washed 3 times
419 for 5 mins with M9 buffer to remove bacteria in their gut. After the third wash animals were
420 plated to regular NGM plates with or without HB101 *E. coli*, and incubated for 4-5 hours before
421 scoring. Animals are scored for the presence of DAF-16::GFP-positive vesicles the intestine
422 using an A1 Zeiss microscope. After 4h-5h of starvation, animals were harvested with M9 buffer
423 from the starved plates and washed once with M9 buffer and plated to NGM plates with HB101
424 *E. coli* and incubated for 1-2 hours at 20°C before scoring.
425
426 **Life span analysis**
427 Replicate strains were maintained for several generations prior to beginning the lifespan assays
428 which were conducted at 20°C. For each strain 25 young adult hermaphrodites were picked to
429 two NGM plates without FUDR seeded with HB101 *E. coli* for three independent replicates
430 totaling 150 animals. Strains were coded and scored blindly to reduce bias. Animals were
431 transferred to fresh NGM plates to avoid contamination and getting crowded out by their
432 progeny. Animals were scored every 2-3 days and were considered dead when they stop
433 exhibiting spontaneous movement and fail to move in response to 1) a gentle touch of the tail, 2)
434 a gentle touch of the head, and 3) gently lifting the head. Animals that die of unnatural causes
435 (internal hatching of embryos, bursting, or crawling off the plate) are omitted. Graphs and

436 statistics were done using Graphpad Prism. None of the strains used in the lifespan assays carry
437 the *fln-2(ot611)* mutation found in a N2 male stock strain and found to extend median lifespan
438 (Gems and Riddle, 2000; Zhao *et al.*, 2019).
439
440 **Fat staining**
441 L4 animals were fixed for staining with Nile Red (Invitrogen) or Oil Red O (Sigma-Aldrich) as
442 previously described (Escorcia *et al.*, 2018). Imaging and analysis was done as previously
443 described (Ratemi *et al.*, 2019). Graphs and statistics were done using Graphpad Prism.
444
445 **Quantitative real-time RT-PCR**
446 *C. elegans* RNA was isolated from young adults maintained at 15°C using TRIZOL reagent
447 (Invitrogen). 1 ug of RNA was reverse transcribed into cDNA using the High-Capacity cDNA
448 Reverse Transcriptase Kit (Applied Biosystems). Quantitative real-time PCR was performed
449 using 1 µl of the cDNA preparation with SYBR-Green Reagents and a Vii7 qPCR analyzer
450 (Applied Biosystems). Each DAF-16 target gene was amplified using PCR primers as described
451 in (Senchuk *et al.*, 2018) and compared to *act-3* (Key Resource Table).
452
453 **Statistical Analysis**
454 Statistical analysis was carried out using GraphPad Prism software. For the analysis of two
455 groups, a student t test was performed using two-tailed distribution for analysis involving two
456 groups of samples. Fishers' exact test was used for comparing groups of four. For each analysis,
457 $P<0.05$ was considered as significant.
458

459

460

461 **ACKNOWLEDGEMENTS**

462 We thank Ali Fazlollahi for technical assistance, Meera Sundaram (University of Pennsylvania)
463 for comments and suggestions, Simon Wing, Richard Roy and Monique Zetka (McGill
464 University) for reagents, Aimee Kao (UCSF) for *muIs113*, Patrick Hu (Vanderbilt University)
465 for the *sgk-1* strains as well as Yanping Zhang, Wenhong Zhang and Meng-Qiu Dong (National
466 Institute of Biological Sciences, Beijing) for generously sharing *daf-16(hq23)* ahead of
467 publication. We thank Wormbase for information on genes and mutations. Some deletion
468 mutations used in this study were provided by the National BioResource Project (Japan) and the
469 International *C. elegans* Gene Knockout Consortium at the Oklahoma Medical Research
470 Foundation, which is funded by the National Institutes of Health (NIH); and the University of
471 British Columbia, which is funded by the Canadian Institute for Health Research (CIHR),
472 Genome Canada, Genome B.C., the Michael Smith Foundation, and the NIH. Some strains were
473 provided by the CGC, which is funded by NIH Office of Research Infrastructure Programs (P40
474 OD010440).

475 FUNDING

476 This work was supported by a CIHR Project Grant (PJT-159725) and in part from the RI-MUHC
477 which receives funding from the Fonds de Recherche du Quebec Santé (FRQS). JVR is
478 supported by the CIHR, the Natural Sciences and Engineering Research Council of Canada
479 (NSERC) and the National Institute of General Medical Sciences (NIGMS; Grant number R01

480 GM121756). JVR received a salary award from the FRQS. TL received a scholarship from
481 FRQS.

482

483 **REFERENCES**

484

485 Accili D, Arden KC (2004). FoxOs at the crossroads of cellular metabolism, differentiation, and
486 transformation. Cell *117*, 421-426.

487 Ackerman D, Gems D (2012). Insulin/IGF-1 and hypoxia signaling act in concert to regulate iron
488 homeostasis in Caenorhabditis elegans. PLoS Genet *8*, e1002498.

489 Aghayeva U, Bhattacharya A, Hobert O (2020). A panel of fluorophore-tagged daf-16 alleles.
490 MicroPubl Biol *2020*.

491 Baass PC, Di Guglielmo GM, Authier F, Posner BI, Bergeron JJ (1995). Compartmentalized
492 signal transduction by receptor tyrosine kinases. Trends Cell Biol *5*, 465-470.

493 Balbis A, Baquiran G, Bergeron JJ, Posner BI (2000). Compartmentalization and insulin-induced
494 translocations of insulin receptor substrates, phosphatidylinositol 3-kinase, and protein kinase B
495 in rat liver. Endocrinology *141*, 4041-4049.

496 Barthel A, Schmoll D, Unterman TG (2005). FoxO proteins in insulin action and metabolism.
497 Trends Endocrinol Metab *16*, 183-189.

498 Baugh LR, Sternberg PW (2006). DAF-16/FOXO regulates transcription of cki-1/Cip/Kip and
499 repression of lin-4 during C. elegans L1 arrest. Curr Biol *16*, 780-785.

500 Behrends C, Sowa ME, Gygi SP, Harper JW (2010). Network organization of the human
501 autophagy system. Nature *466*, 68-76.

502 Bergeron JJ, Di Guglielmo GM, Dahan S, Dominguez M, Posner BI (2016). Spatial and
503 Temporal Regulation of Receptor Tyrosine Kinase Activation and Intracellular Signal
504 Transduction. Annual review of biochemistry *85*, 573-597.
505 Berman JR, Kenyon C (2006). Germ-cell loss extends C. elegans life span through regulation of
506 DAF-16 by kri-1 and lipophilic-hormone signaling. Cell *124*, 1055-1068.
507 Bhattacharya A, Aghayeva U, Berghoff EG, Hobert O (2019). Plasticity of the Electrical
508 Connectome of C. elegans. Cell *176*, 1174-1189 e1116.
509 Braccini L, Ciraolo E, Campa CC, Perino A, Longo DL, Tibolla G, Pregnolato M, Cao Y,
510 Tassone B, Damilano F*, et al.* (2015). PI3K-C2gamma is a Rab5 effector selectively controlling
511 endosomal Akt2 activation downstream of insulin signalling. Nat Commun *6*, 7400.
512 Brunet A, Bonni A, Zigmond MJ, Lin MZ, Juo P, Hu LS, Anderson MJ, Arden KC, Blenis J,
513 Greenberg ME (1999). Akt promotes cell survival by phosphorylating and inhibiting a Forkhead
514 transcription factor. Cell *96*, 857-868.
515 Carroll B, Mohd-Naim N, Maximiano F, Frasa MA, McCormack J, Finelli M, Thoresen SB,
516 Perdios L, Daigaku R, Francis RE*, et al.* (2013). The TBC/RabGAP Armus coordinates Rac1
517 and Rab7 functions during autophagy. Dev Cell *25*, 15-28.
518 Chavrier P, Parton RG, Hauri HP, Simons K, Zerial M (1990). Localization of low molecular
519 weight GTP binding proteins to exocytic and endocytic compartments. Cell *62*, 317-329.
520 Chen CC, Schweinsberg PJ, Vashist S, Mareiniss DP, Lambie EJ, Grant BD (2006). RAB-10 Is
521 Required for Endocytic Recycling in the Caenorhabditis elegans Intestine. Mol Biol Cell *17*,
522 1286-1297.

523 Cheng KK, Iglesias MA, Lam KS, Wang Y, Sweeney G, Zhu W, Vanhoutte PM, Kraegen EW,
524 Xu A (2009). APPL1 potentiates insulin-mediated inhibition of hepatic glucose production and
525 alleviates diabetes via Akt activation in mice. Cell Metab *9*, 417-427.
526 Chotard L, Mishra AK, Sylvain MA, Tuck S, Lambright DG, Rocheleau CE (2010a). TBC-2
527 regulates RAB-5/RAB-7-mediated endosomal trafficking in Caenorhabditis elegans. Mol Biol
528 Cell *21*, 2285-2296.
529 Chotard L, Skorobogata O, Sylvain MA, Shrivastava S, Rocheleau CE (2010b). TBC-2 is
530 required for embryonic yolk protein storage and larval survival during L1 diapause in
531 Caenorhabditis elegans. PLoS One *5*, e15662.
532 Christoforidis S, Miaczynska M, Ashman K, Wilm M, Zhao L, Yip SC, Waterfield MD, Backer
533 JM, Zerial M (1999). Phosphatidylinositol-3-OH kinases are Rab5 effectors. Nat Cell Biol *1*,
534 249-252.
535 Clokey GV, Jacobson LA (1986). The autofluorescent "lipofuscin granules" in the intestinal cells
536 of Caenorhabditis elegans are secondary lysosomes. Mech Ageing Dev *35*, 79-94.
537 Coburn C, Allman E, Mahanti P, Benedetto A, Cabreiro F, Pincus Z, Matthijssens F, Araiz C,
538 Mandel A, Vlachos M*, et al.* (2013). Anthranilate fluorescence marks a calcium-propagated
539 necrotic wave that promotes organismal death in C. elegans. PLoS Biol *11*, e1001613.
540 Escorcia W, Ruter DL, Nhan J, Curran SP (2018). Quantification of Lipid Abundance and
541 Evaluation of Lipid Distribution in Caenorhabditis elegans by Nile Red and Oil Red O Staining.
542 J Vis Exp.
543 Fraser AG, Kamath RS, Zipperlen P, Martinez-Campos M, Sohrmann M, Ahringer J (2000).
544 Functional genomic analysis of C. elegans chromosome I by systematic RNA interference.
545 Nature *408*, 325-330.

546 Gems D, Riddle DL (2000). Defining wild-type life span in Caenorhabditis elegans. J Gerontol
547 A Biol Sci Med Sci *55*, B215-219.
548 Greer EL, Brunet A (2005). FOXO transcription factors at the interface between longevity and
549 tumor suppression. Oncogene *24*, 7410-7425.
550 Greer EL, Dowlatshahi D, Banko MR, Villen J, Hoang K, Blanchard D, Gygi SP, Brunet A
551 (2007). An AMPK-FOXO pathway mediates longevity induced by a novel method of dietary
552 restriction in C. elegans. Curr Biol *17*, 1646-1656.
553 Guo B, Huang X, Zhang P, Qi L, Liang Q, Zhang X, Huang J, Fang B, Hou W, Han J*, et al.*
554 (2014). Genome-wide screen identifies signaling pathways that regulate autophagy during
555 Caenorhabditis elegans development. EMBO Rep *15*, 705-713.
556 Hars ES, Qi H, Ryazanov AG, Jin S, Cai L, Hu C, Liu LF (2007). Autophagy regulates ageing in
557 C. elegans. Autophagy *3*, 93-95.
558 Henderson ST, Johnson TE (2001). daf-16 integrates developmental and environmental inputs to
559 mediate aging in the nematode Caenorhabditis elegans. Curr Biol *11*, 1975-1980.
560 Hermann GJ, Schroeder LK, Hieb CA, Kershner AM, Rabbitts BM, Fonarev P, Grant BD, Priess
561 JR (2005). Genetic analysis of lysosomal trafficking in Caenorhabditis elegans. Mol Biol Cell
562 *16*, 3273-3288.
563 Hertweck M, Gobel C, Baumeister R (2004). C. elegans SGK-1 is the critical component in the
564 Akt/PKB kinase complex to control stress response and life span. Dev Cell *6*, 577-588.
565 Honda Y, Honda S (1999). The daf-2 gene network for longevity regulates oxidative stress
566 resistance and Mn-superoxide dismutase gene expression in Caenorhabditis elegans. FASEB
567 journal : official publication of the Federation of American Societies for Experimental Biology
568 *13*, 1385-1393.

569 Hsu JW, Bai M, Li K, Yang JS, Chu N, Cole PA, Eck MJ, Li J, Hsu VW (2020). The protein
570 kinase Akt acts as a coat adaptor in endocytic recycling. Nat Cell Biol *22*, 927-933.
571 Huotari J, Helenius A (2011). Endosome maturation. EMBO J *30*, 3481-3500.
572 Jones KT, Greer ER, Pearce D, Ashrafi K (2009). Rictor/TORC2 regulates Caenorhabditis
573 elegans fat storage, body size, and development through sgk-1. PLoS Biol *7*, e60.
574 Jungmichel S, Sylvestersen KB, Choudhary C, Nguyen S, Mann M, Nielsen ML (2014).
575 Specificity and commonality of the phosphoinositide-binding proteome analyzed by quantitative
576 mass spectrometry. Cell Rep *6*, 578-591.
577 Kamath RS, Fraser AG, Dong Y, Poulin G, Durbin R, Gotta M, Kanapin A, Le Bot N, Moreno
578 S, Sohrmann M*, et al.* (2003). Systematic functional analysis of the Caenorhabditis elegans
579 genome using RNAi. Nature *421*, 231-237.
580 Kamath RS, Martinez-Campos M, Zipperlen P, Fraser AG, Ahringer J (2001). Effectiveness of
581 specific RNA-mediated interference through ingested double-stranded RNA in Caenorhabditis
582 elegans. Genome Biol *2*, RESEARCH0002.
583 Kang C, Xu Q, Martin TD, Li MZ, Demaria M, Aron L, Lu T, Yankner BA, Campisi J, Elledge
584 SJ (2015). The DNA damage response induces inflammation and senescence by inhibiting
585 autophagy of GATA4. Science *349*, aaa5612.
586 Kenyon C, Chang J, Gensch E, Rudner A, Tabtiang R (1993). A C. elegans mutant that lives
587 twice as long as wild type. Nature *366*, 461-464.
588 Khan MN, Savoie S, Bergeron JJ, Posner BI (1986). Characterization of rat liver endosomal
589 fractions. In vivo activation of insulin-stimulable receptor kinase in these structures. J Biol Chem
590 *261*, 8462-8472.

591 Kim Y, Shiba-Ishii A, Nakagawa T, Iemura SI, Natsume T, Nakano N, Matsuoka R, Sakashita S,
592 Lee S, Kawaguchi A*, et al.* (2018). Stratifin regulates stabilization of receptor tyrosine kinases
593 via interaction with ubiquitin-specific protease 8 in lung adenocarcinoma. Oncogene *37*, 5387-
594 5402.
595 Kimura KD, Tissenbaum HA, Liu Y, Ruvkun G (1997). daf-2, an insulin receptor-like gene that
596 regulates longevity and diapause in Caenorhabditis elegans. Science *277*, 942-946.
597 Kwon ES, Narasimhan SD, Yen K, Tissenbaum HA (2010). A new DAF-16 isoform regulates
598 longevity. Nature *466*, 498-502.
599 Lapierre LR, De Magalhaes Filho CD, McQuary PR, Chu CC, Visvikis O, Chang JT, Gelino S,
600 Ong B, Davis AE, Irazoqui JE*, et al.* (2013). The TFEB orthologue HLH-30 regulates autophagy
601 and modulates longevity in Caenorhabditis elegans. Nature communications *4*, 2267.
602 Law F, Seo JH, Wang Z, DeLeon JL, Bolis Y, Brown A, Zong WX, Du G, Rocheleau CE
603 (2017). The VPS34 PI3K negatively regulates RAB-5 during endosome maturation. J Cell Sci
604 *130*, 2007-2017.
605 Li W, Zou W, Zhao D, Yan J, Zhu Z, Lu J, Wang X (2009). C. elegans Rab GTPase activating
606 protein TBC-2 promotes cell corpse degradation by regulating the small GTPase RAB-5.
607 Development *136*, 2445-2455.
608 Libina N, Berman JR, Kenyon C (2003). Tissue-specific activities of C. elegans DAF-16 in the
609 regulation of lifespan. Cell *115*, 489-502.
610 Lin K, Dorman JB, Rodan A, Kenyon C (1997). daf-16: An HNF-3/forkhead family member that
611 can function to double the life-span of Caenorhabditis elegans. Science *278*, 1319-1322.
612 Lin K, Hsin H, Libina N, Kenyon C (2001). Regulation of the Caenorhabditis elegans longevity
613 protein DAF-16 by insulin/IGF-1 and germline signaling. Nat Genet *28*, 139-145.

614 Liu O, Grant BD (2015). Basolateral Endocytic Recycling Requires RAB-10 and AMPH-1
615 Mediated Recruitment of RAB-5 GAP TBC-2 to Endosomes. PLoS Genet *11*, e1005514.
616 Marat AL, Wallroth A, Lo WT, Muller R, Norata GD, Falasca M, Schultz C, Haucke V (2017).
617 mTORC1 activity repression by late endosomal phosphatidylinositol 3,4-bisphosphate. Science
618 *356*, 968-972.
619 Melendez A, Talloczy Z, Seaman M, Eskelinen EL, Hall DH, Levine B (2003). Autophagy genes
620 are essential for dauer development and life-span extension in C. elegans. Science *301*, 1387-
621 1391.
622 Miaczynska M (2013). Effects of membrane trafficking on signaling by receptor tyrosine
623 kinases. Cold Spring Harbor perspectives in biology *5*, a009035.
624 Mondin VE, Ben El Kadhi K, Cauvin C, Jackson-Crawford A, Belanger E, Decelle B, Salomon
625 R, Lowe M, Echard A, Carreno S (2019). PTEN reduces endosomal PtdIns(4,5)P2 in a
626 phosphatase-independent manner via a PLC pathway. J Cell Biol *218*, 2198-2214.
627 Morton DG, Shakes DC, Nugent S, Dichoso D, Wang W, Golden A, Kemphues KJ (2002). The
628 Caenorhabditis elegans par-5 gene encodes a 14-3-3 protein required for cellular asymmetry in
629 the early embryo. Dev Biol *241*, 47-58.
630 Munoz MJ, Riddle DL (2003). Positive selection of Caenorhabditis elegans mutants with
631 increased stress resistance and longevity. Genetics *163*, 171-180.
632 Murphy CT, Hu PJ (2013). Insulin/insulin-like growth factor signaling in C. elegans.
633 WormBook, 1-43.
634 Murphy CT, McCarroll SA, Bargmann CI, Fraser A, Kamath RS, Ahringer J, Li H, Kenyon C
635 (2003). Genes that act downstream of DAF-16 to influence the lifespan of Caenorhabditis
636 elegans. Nature *424*, 277-283.

637 Naguib A, Bencze G, Cho H, Zheng W, Tocilj A, Elkayam E, Faehnle CR, Jaber N, Pratt CP,
638 Chen M*, et al.* (2015). PTEN functions by recruitment to cytoplasmic vesicles. Mol Cell *58*, 255-
639 268.
640 O'Rourke EJ, Soukas AA, Carr CE, Ruvkun G (2009). C. elegans major fats are stored in
641 vesicles distinct from lysosome-related organelles. Cell Metab *10*, 430-435.
642 Ogg S, Paradis S, Gottlieb S, Patterson GI, Lee L, Tissenbaum HA, Ruvkun G (1997). The Fork
643 head transcription factor DAF-16 transduces insulin-like metabolic and longevity signals in C.
644 elegans. Nature *389*, 994-999.
645 Ogg S, Ruvkun G (1998). The C. elegans PTEN homolog, DAF-18, acts in the insulin receptor-
646 like metabolic signaling pathway. Mol Cell *2*, 887-893.
647 Oh SW, Mukhopadhyay A, Svrzikapa N, Jiang F, Davis RJ, Tissenbaum HA (2005). JNK
648 regulates lifespan in Caenorhabditis elegans by modulating nuclear translocation of forkhead
649 transcription factor/DAF-16. Proc Natl Acad Sci U S A *102*, 4494-4499.
650 Paradis S, Ruvkun G (1998). Caenorhabditis elegans Akt/PKB transduces insulin receptor-like
651 signals from AGE-1 PI3 kinase to the DAF-16 transcription factor. Genes Dev *12*, 2488-2498.
652 Popovic D, Akutsu M, Novak I, Harper JW, Behrends C, Dikic I (2012). Rab GTPase-activating
653 proteins in autophagy: regulation of endocytic and autophagy pathways by direct binding to
654 human ATG8 modifiers. Mol Cell Biol *32*, 1733-1744.
655 Ratemi Z, Kiss R, Rocheleau C (2019). C. elegans rab-18 mutants display reduced lipid content
656 under fed and fasted conditions. MicroPubl Biol *2019*.
657 Riddle DL, Swanson MM, Albert PS (1981). Interacting genes in nematode dauer larva
658 formation. Nature *290*, 668-671.

659 Robida-Stubbs S, Glover-Cutter K, Lamming DW, Mizunuma M, Narasimhan SD, Neumann-
660 Haefelin E, Sabatini DM, Blackwell TK (2012). TOR signaling and rapamycin influence
661 longevity by regulating SKN-1/Nrf and DAF-16/FoxO. Cell Metab *15*, 713-724.
662 Ruck A, Attonito J, Garces KT, Nunez L, Palmisano NJ, Rubel Z, Bai Z, Nguyen KC, Sun L,
663 Grant BD*, et al.* (2011). The Atg6/Vps30/Beclin 1 ortholog BEC-1 mediates endocytic
664 retrograde transport in addition to autophagy in C. elegans. Autophagy *7*, 386-400.
665 Samuelson AV, Carr CE, Ruvkun G (2007). Gene activities that mediate increased life span of
666 C. elegans insulin-like signaling mutants. Genes Dev *21*, 2976-2994.
667 Sancak Y, Peterson TR, Shaul YD, Lindquist RA, Thoreen CC, Bar-Peled L, Sabatini DM
668 (2008). The Rag GTPases bind raptor and mediate amino acid signaling to mTORC1. Science
669 *320*, 1496-1501.
670 Sasidharan N, Sumakovic M, Hannemann M, Hegermann J, Liewald JF, Olendrowitz C, Koenig
671 S, Grant BD, Rizzoli SO, Gottschalk A*, et al.* (2012). RAB-5 and RAB-10 cooperate to regulate
672 neuropeptide release in Caenorhabditis elegans. Proc Natl Acad Sci U S A *109*, 18944-18949.
673 Sato M, Sato K, Fonarev P, Huang CJ, Liou W, Grant BD (2005). Caenorhabditis elegans RME-
674 6 is a novel regulator of RAB-5 at the clathrin-coated pit. Nat Cell Biol *7*, 559-569.
675 Schenck A, Goto-Silva L, Collinet C, Rhinn M, Giner A, Habermann B, Brand M, Zerial M
676 (2008). The endosomal protein Appl1 mediates Akt substrate specificity and cell survival in
677 vertebrate development. Cell *133*, 486-497.
678 Senchuk MM, Dues DJ, Schaar CE, Johnson BK, Madaj ZB, Bowman MJ, Winn ME, Van
679 Raamsdonk JM (2018). Activation of DAF-16/FOXO by reactive oxygen species contributes to
680 longevity in long-lived mitochondrial mutants in Caenorhabditis elegans. PLoS Genet *14*,
681 e1007268.

682 Settembre C, Fraldi A, Medina DL, Ballabio A (2013). Signals from the lysosome: a control
683 centre for cellular clearance and energy metabolism. Nat Rev Mol Cell Biol *14*, 283-296.
684 Shin HW, Hayashi M, Christoforidis S, Lacas-Gervais S, Hoepfner S, Wenk MR, Modregger J,
685 Uttenweiler-Joseph S, Wilm M, Nystuen A*, et al.* (2005). An enzymatic cascade of Rab5
686 effectors regulates phosphoinositide turnover in the endocytic pathway. J Cell Biol *170*, 607-618.
687 Shinde SR, Maddika S (2016). PTEN modulates EGFR late endocytic trafficking and
688 degradation by dephosphorylating Rab7. Nature communications *7*, 10689.
689 Shinde SR, Maddika S (2017). PTEN Regulates Glucose Transporter Recycling by Impairing
690 SNX27 Retromer Assembly. Cell Rep *21*, 1655-1666.
691 Su X, Lodhi IJ, Saltiel AR, Stahl PD (2006). Insulin-stimulated Interaction between insulin
692 receptor substrate 1 and p85alpha and activation of protein kinase B/Akt require Rab5. J Biol
693 Chem *281*, 27982-27990.
694 Sun L, Liu O, Desai J, Karbassi F, Sylvain MA, Shi A, Zhou Z, Rocheleau CE, Grant BD
695 (2012). CED-10/Rac1 regulates endocytic recycling through the RAB-5 GAP TBC-2. PLoS
696 Genet *8*, e1002785.
697 Sun X, Chen WD, Wang YD (2017). DAF-16/FOXO Transcription Factor in Aging and
698 Longevity. Front Pharmacol *8*, 548.
699 Sun Y, Li M, Zhao D, Li X, Yang C, Wang X (2020). Lysosome activity is modulated by
700 multiple longevity pathways and is important for lifespan extension in C. elegans. Elife *9*.
701 Swanson MM, Riddle DL (1981). Critical periods in the development of the Caenorhabditis
702 elegans dauer larva. Dev Biol *84*, 27-40.

703 Tepper RG, Ashraf J, Kaletsky R, Kleemann G, Murphy CT, Bussemaker HJ (2013). PQM-1
704 complements DAF-16 as a key transcriptional regulator of DAF-2-mediated development and
705 longevity. Cell *154*, 676-690.
706 Timmons L, Fire A (1998). Specific interference by ingested dsRNA. Nature *395*, 854.
707 Toyofuku T, Morimoto K, Sasawatari S, Kumanogoh A (2015). Leucine-Rich Repeat Kinase 1
708 Regulates Autophagy through Turning On TBC1D2-Dependent Rab7 Inactivation. Mol Cell Biol
709 *35*, 3044-3058.
710 Walz HA, Shi X, Chouinard M, Bue CA, Navaroli DM, Hayakawa A, Zhou QL, Nadler J,
711 Leonard DM, Corvera S (2010). Isoform-specific regulation of Akt signaling by the endosomal
712 protein WDFY2. J Biol Chem *285*, 14101-14108.
713 Wang W, Shakes DC (1997). Expression patterns and transcript processing of ftt-1 and ftt-2, two
714 C. elegans 14-3-3 homologues. J Mol Biol *268*, 619-630.
715 Wang Y, Oh SW, Deplancke B, Luo J, Walhout AJ, Tissenbaum HA (2006). C. elegans 14-3-3
716 proteins regulate life span and interact with SIR-2.1 and DAF-16/FOXO. Mech Ageing Dev *127*,
717 741-747.
718 Zeigerer A, Bogorad RL, Sharma K, Gilleron J, Seifert S, Sales S, Berndt N, Bulik S, Marsico G,
719 D'Souza RCJ*, et al.* (2015). Regulation of liver metabolism by the endosomal GTPase Rab5. Cell
720 Rep *11*, 884-892.
721 Zhang Y-P, Zhang W-H, Zhang P, Li Q, Sun Y, Wang J-W, Zhang S-BO, Cai T, Zhan C, Dong
722 M-Q (2021). Degrading intestinal DAF-2 nearly doubles *Caenorhabditis elegans* lifespan
723 without affecting development or reproduction. bioRxiv.
724 Zhao Y, Wang H, Poole RJ, Gems D (2019). A fln-2 mutation affects lethal pathology and
725 lifespan in C. elegans. Nature communications *10*, 5087.

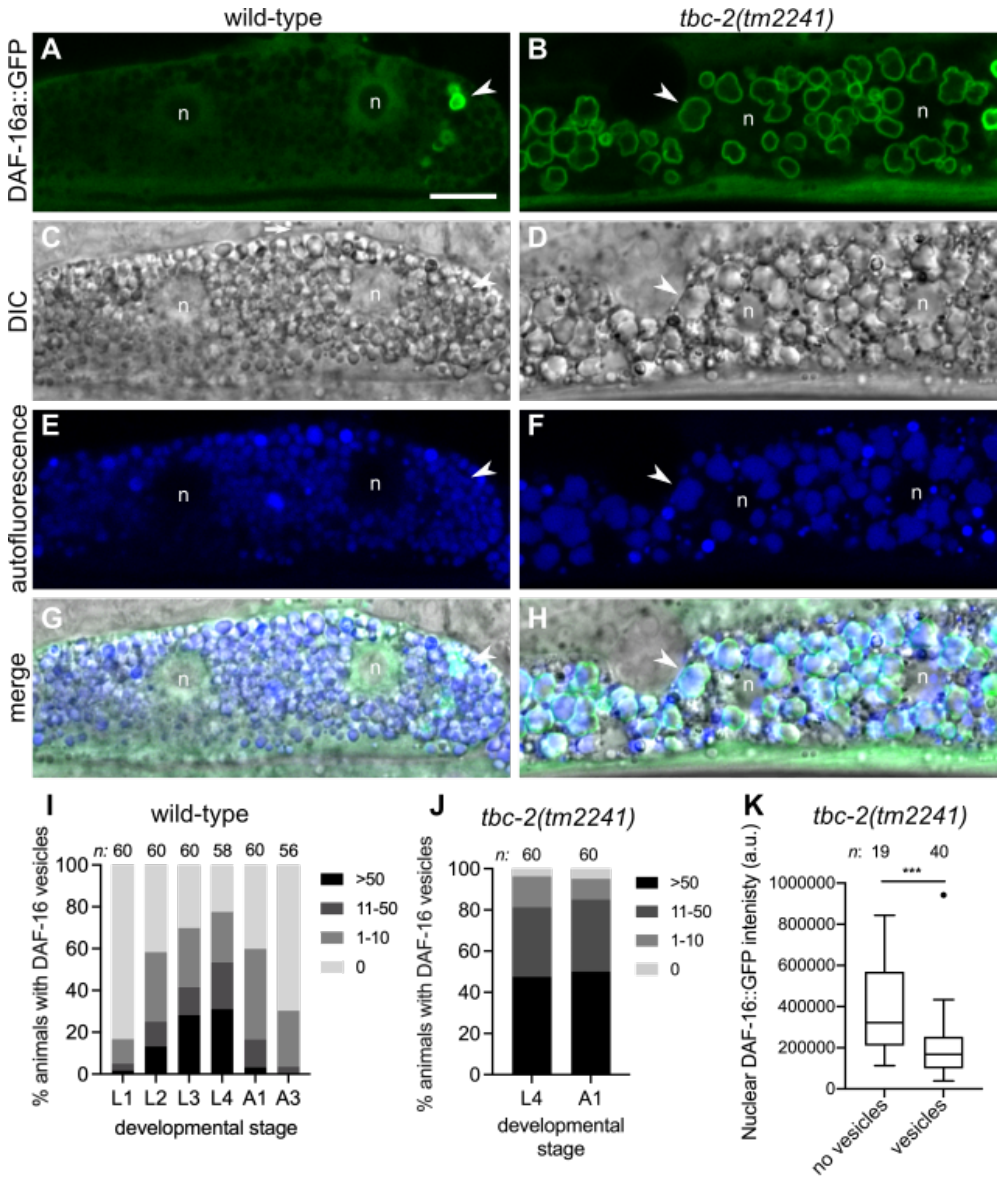

728

729 **Figure 1. DAF-16 FOXO localizes to vesicles in intestinal cells**

730 (A-H) Representative confocal and differential interference contrast (DIC) images of an

731 intestinal cell of wild-type (A, C, E, G) and *tbc-2(tm2241)* (B, D, F, H) animals expressing

732 DAF-16a::GFP *(zIs356)*. DAF-16a::GFP (green) is present on vesicles in both wild-type and

733 *tbc-2(tm2241)* intestinal cells (A and B) that are positive for autofluorescence (blue) present in

734 the the endolysosomal system (E and F). Corresponding DIC (C and D) and merged (G and F)

735 images are shown. A representative vesicle is shown (arrow head) and the two nuclei of the

736 binucleate cell are marked (n). Note that DAF-16a::GFP is excluded from the large nucleoli (A).
737 (I-J) Grouped bar graphs quantifying the percentage of wild-type (I) and *tbc-2(tm2241)* (J)
738 animals with 0, 1-10, 11-50 or >50 DAF-16a::GFP *(zIs356)* positive vesicles at the different
739 larval stages (L1-4) or 1 and 3 day old adults (A1 and A3). (K) A Tukey boxplot of the nuclear
740 intensity in artificial units (a.u.) of DAF-16a::GFP in *tbc-2(tm2241)* intestinal cells with and
741 without DAF-16a::GFP positive vesicles. *n,* total number of animals *** $P<0.001$ in an unpaired
742 t test (Prism 8). Scale bar (A), 10µm.
743

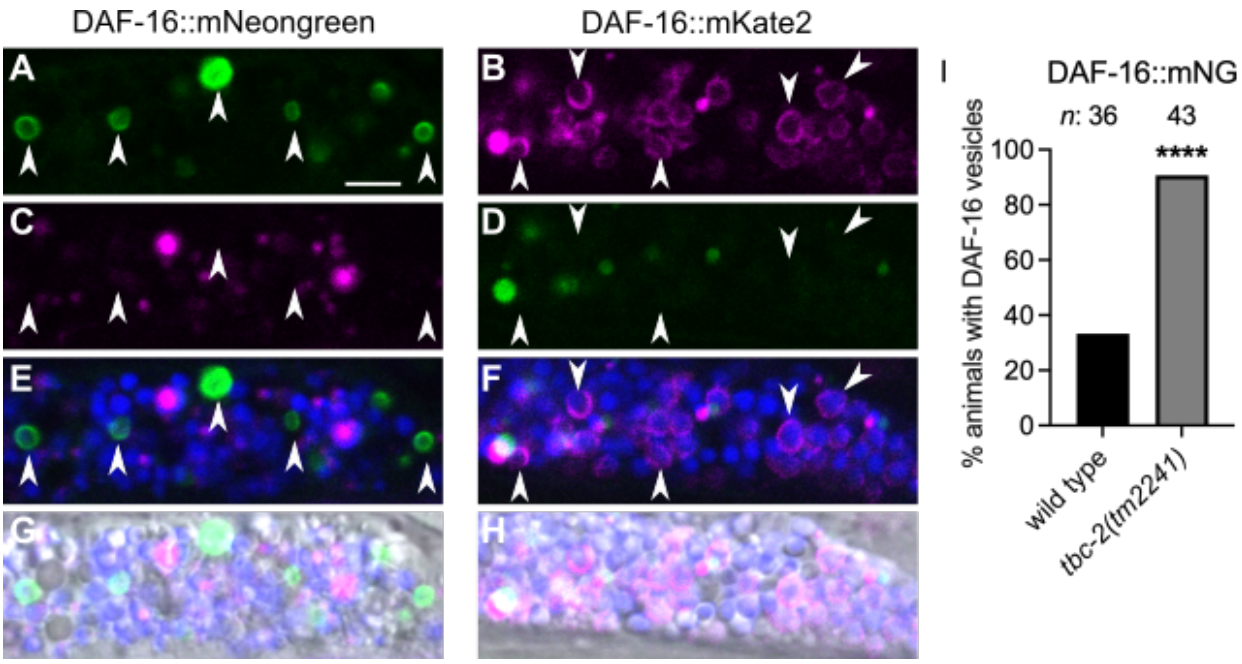

Figure 2. Endogenously tagged DAF-16::mNeongreen and DAF-16 ::mKate2 localize to vesicles. Representative confocal and differential interference contrast (DIC) images of intestinal cells of *daf-16(ot853[daf-16::linker::mNeongreen::3xFlag::AID])* (A,C,E,G) and *daf-16(ot821[daf-16::mKate2::3xFlag])* (B,D,F,H). Arrows mark DAF-16::mNeongreen positive vesicles in the green channel (A) that are distinct from autofluorescence in the red (C) and blue channels shown as a merge (E). Arrows mark DAF-16::mKate2 positive vesicles in the red channel (B) that are distinct from autofluorescence in the green (D) and blue channels shown as a merge (F). For additional context the fluorescent channels were merged with their corresponding DIC image (G and H). Bar graphs displaying the percent wild-type and *tbc-2(tm2241)* animals with DAF-16::mNG positive vesicles (I). Fisher's exact test (graphpad.com) was used to determine the statistical difference between conditions. *n*, total number of animals. **** *P<0.0001.* Scale bar (A), 5µm.

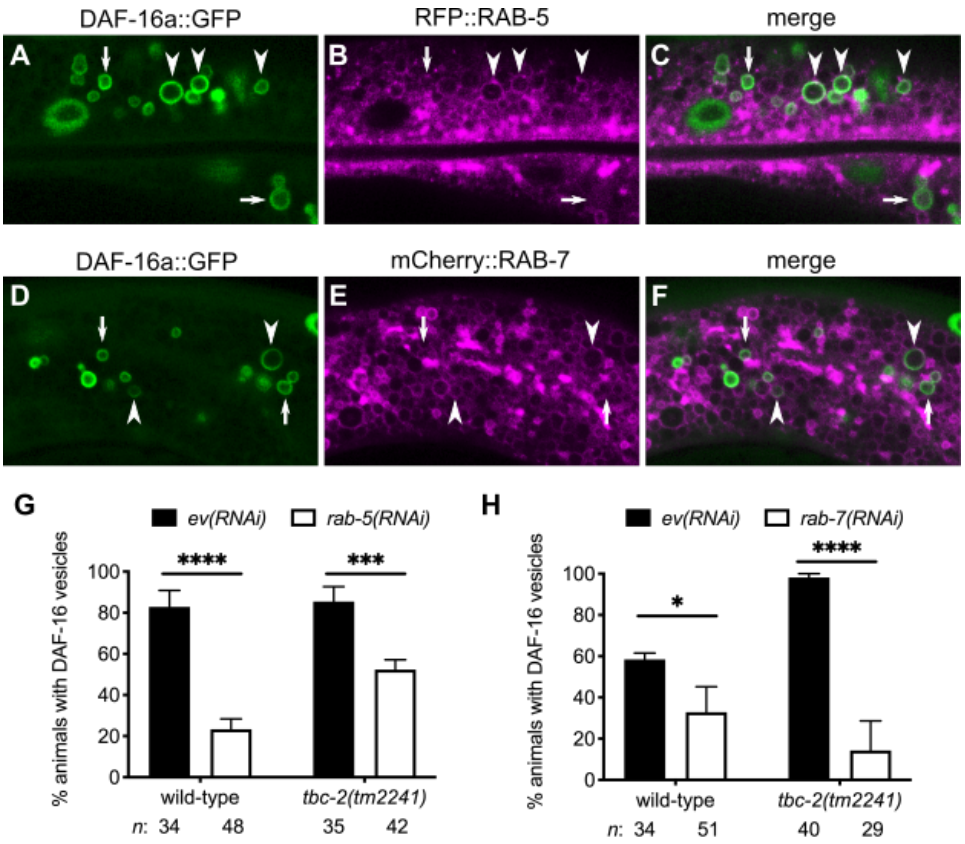

Figure 3. RAB-5 and RAB-7 GTPases promote DAF-16 FOXO localization to endosomes

(A-F) Representative confocal images of the intestinal cells of animals expressing DAF-16a::GFP (*zIs356)* (green) and either RFP::RAB-5 (*pwIs480*) (A-C) or mCherry::RAB-7 (*pwIs429*) (magenta) (D- F). Arrowheads mark examples of vesicles positive for both DAF-16a::GFP and either RFP::RAB-5 or mCherry::RAB-7. Arrows mark examples of DAF-16a::GFP vesicles that are not positive for either RFP::RAB-5 or mCherry::RAB-7. (G and H) Bar graphs displaying the mean (and SEM) of the percent wild-type and *tbc-2(tm2241)* animals with DAF-16a::GFP (*zIs356*) vesicles fed bacteria expressing control empty vector (ev) RNAi (black bars) compared to animals fed *rab-5(RNAi)* or *rab-7(RNAi)* (white bars) from three independent experiments. Fisher's exact test (graphpad.com) was used to determine the statistical difference between conditions. *n*, total number of animals. * *P<0.05, *** P<0.001, **** P<0.0001.*

772

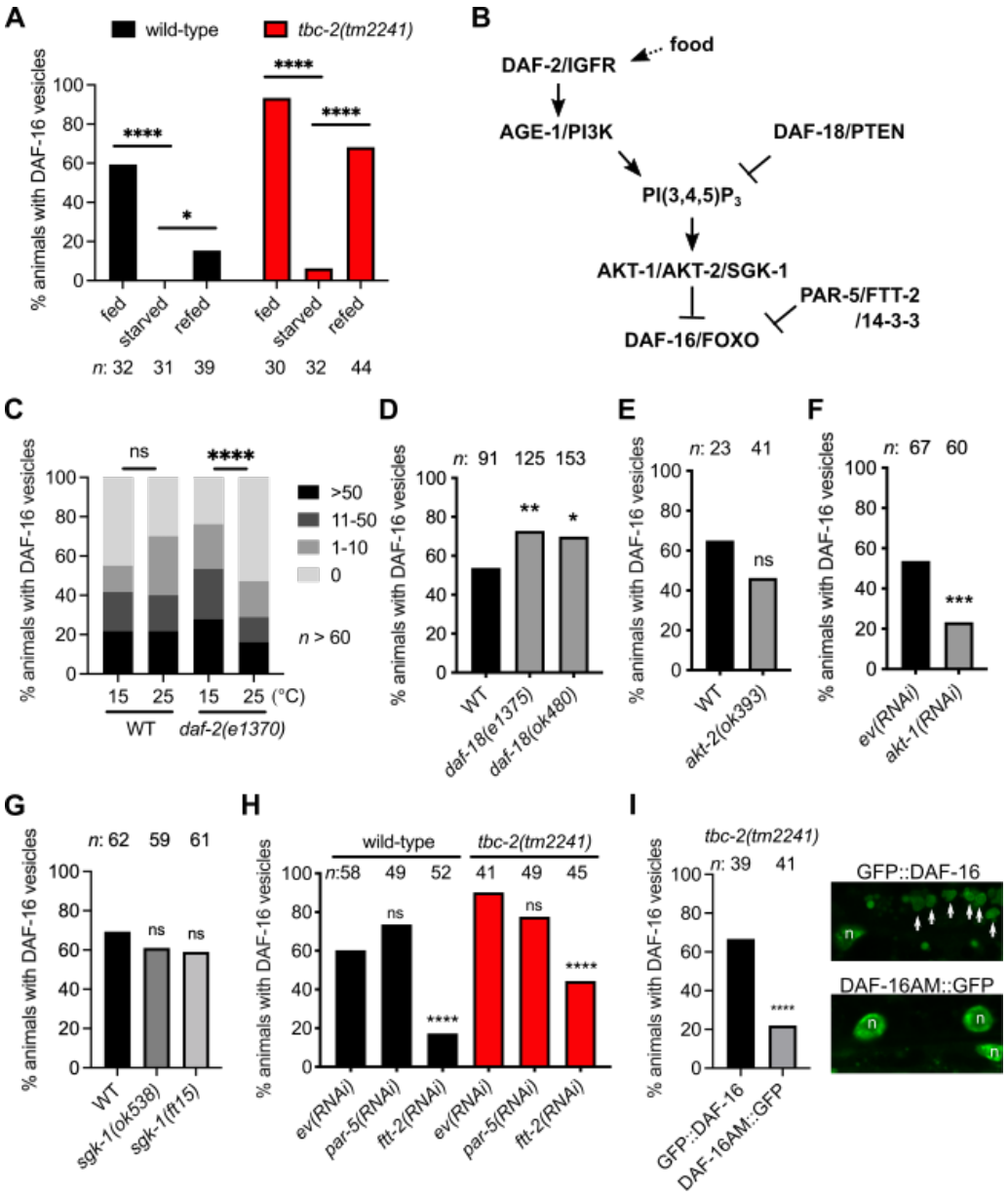

773

774 **Figure 4. DAF-16 FOXO endosome localization is regulated by IIS and nutrient availability**

775 (A) Bar graphs of the percent wild-type (black) and *tbc-2(tm2241)* (red) animals with DAF-

776 16a::GFP (*zIs356*) vesicles in fed animals, animals starved between 4 and 5 hours and starved

777 animals that have been refed for 1 to 2 hours. (B) Diagram of IIS-mediate regulation of DAF-

778 16/FOXO. (C) Grouped bar graphs quantifying the percentage of wild-type and *daf-2(e1370)* L4

779 larvae (cumulative data from 3 independent strains) with 0, 1-10, 11-50 or >50 DAF-16a::GFP
780 *(zIs356)* positive vesicles at 15°C or shifted overnight to 25°C. (D) Bar graphs of percent wild-
781 type and *daf-18(e1375)* (cumulative data from 3 independent strains) and *daf-18(ok480)*
782 (cumulative data from 5 independent strains) with DAF-16a::GFP (*zIs356*) vesicles. (E) Bar
783 graphs of percent wild-type and *akt-2(ok393)* (cumulative data from 2 independent strains) with
784 DAF-16a::GFP (*zIs356*) vesicles. (F) Bar graphs of percent wild-type animals treated with
785 control empty vector RNAi and *akt-1(RNAi)* with DAF-16a::GFP (*zIs356*) vesicles. (G) Bar
786 graphs of percent wild-type, *sgk-1(ok538)* and *sgk-1(ft15)* with DAF-16a::GFP (*zIs356*) vesicles.
787 (H) Bar graphs of the percent wild-type (black) and *tbc-2(tm2241)* (red) animals fed control
788 empty vector RNAi, *par-5(RNAi)* and *ftt-2(RNAi)* with DAF-16a::GFP (*zIs356*) vesicles. (I) Bar
789 graph of the precent *tbc-2(tm2241)* animals with GFP::DAF-16a (*muIs71*) or DAF-16a^{AM}::GFP
790 *(muIs113)*-positive vesicles. Representative images of GFP::DAF-16a (*muIs71*) (top) and DAF-
791 16a^{AM}::GFP *(muIs113)* (bottom) are shown. GFP::DAF-16a vesicles (arrows) and the nuclei (n).
792 Fisher's exact test (graphpad.com) was used to determine the statistical difference between
793 conditions. *n*, total number of animals. ns, not significant, * *P<0.05, ** P<0.01, *** P<0.001,*
794 ***** P<0.0001.*
795
796
797
798

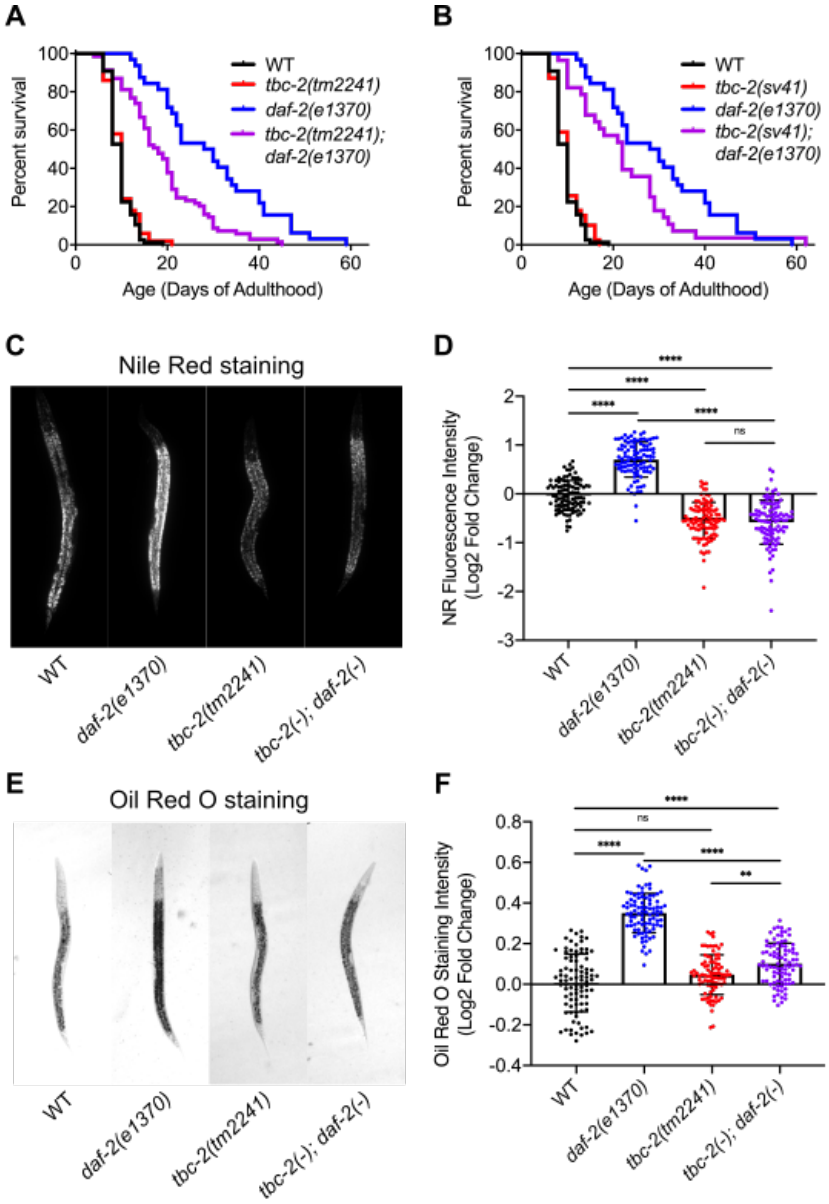

Figure 5. TBC-2 is required for full lifespan extension and increased fat storage resulting from decreased insulin/IGF signaling

(A,B) Percent survival curve of adult animals of wild-type and *daf-2(e1370)* with either *tbc-2(tm2241)* and *tbc-2(tm2241); daf-2(e1370)* (A) or *tbc-2(sv41)* and *tbc-2(sv41); daf-2(e1370)* (B) genotypes. The survival of all strains are statistically different from *daf-2(e1370)* animals as determined by a Mantel-Cox log-rank test: *tbc-2(tm2241); daf-2(e1370)* ($P<0.001$) and *tbc-2(sv41); daf-2(e1370)* ($P=0.0314$). Cumulative data from three independent replicates of 50

806 young adults for a total of 150. (C,D) Log2 fold change in Nile Red (NR) fluorescence intensity
807 (C) or Oil Red O staining intensity (D) comparing wild-type, *daf-2(e1370)*, *tbc-2(tm2241)* and
808 *tbc-2(tm2241); daf-2(e1370)* fixed L4 hermaphrodites. Statistical analysis was done using a
809 student's t-test with a one way analysis of variance (ANOVA). ns, not significant. ** P <0.01,
810 **** P <0.0001.

811

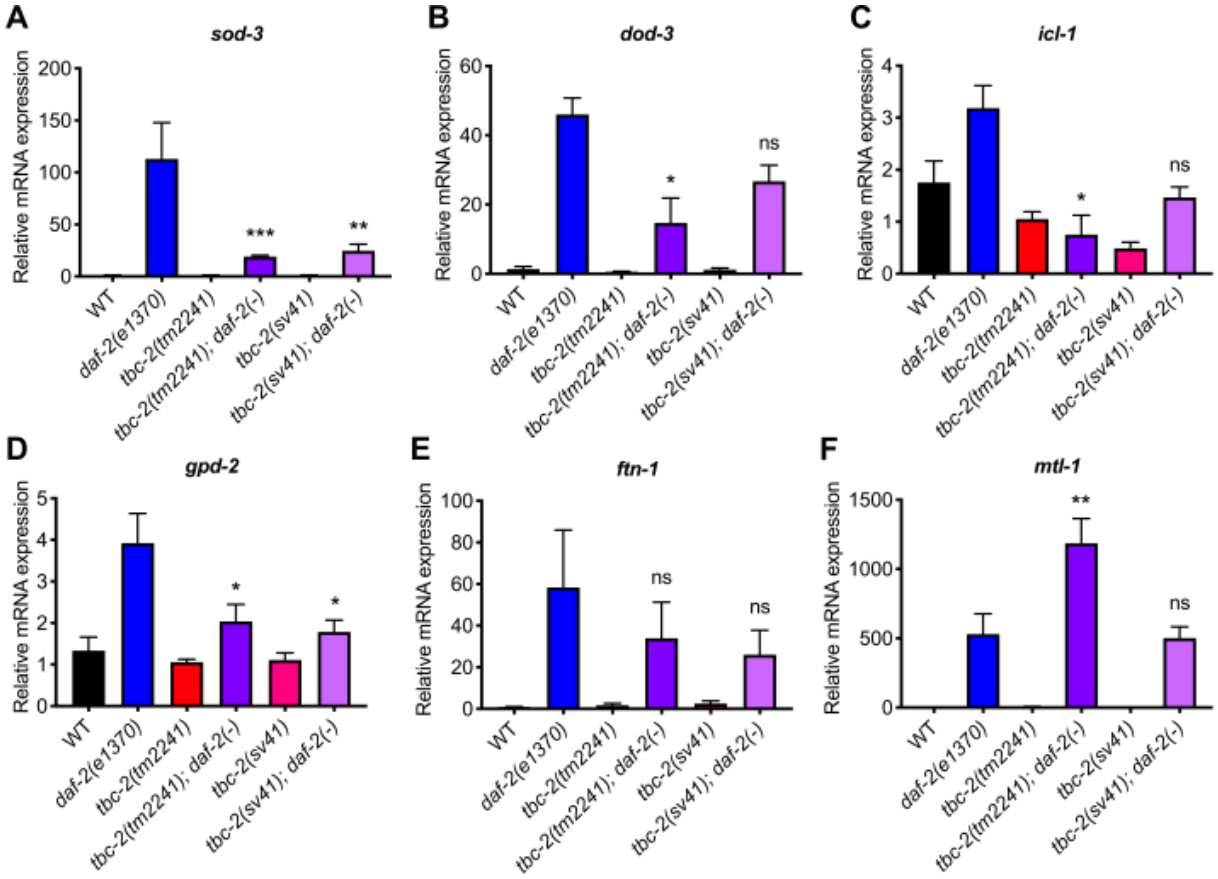

812

813 **Figure 6. TBC-2 is required for the increased DAF-16 target gene expression resulting**
814 **from decreased insulin/IGF signaling**

815 Quantitative RT-PCR analysis of DAF-16 target gene expression in wild-type, *daf-2(e1370)*, *tbc-*
816 *2(tm2241), tbc-2(tm2241); daf-2(e1370), tbc-2(sv41),* and *tbc-2(sv41); daf-2(e1370).* Statistical
817 analysis was performed using an Ordinary one-way ANOVA – Tukey's multiple comparisons

818 test. Shown are comparisons of *tbc-2(tm2241); daf-2(e1370)* and *tbc-2(sv41); daf-2(e1370)*

819 versus *daf-2(e1370)* single mutants. ns, not significant. *p<0.05, **p<0.01, ***p<0.001.

820

821

822